LANGMUIR



pubs.acs.org/Langmuir
Article

# Uncovering Molecular and Kinetic Insights into the Art of Catalyst Synthesis by Strong Electrostatic Adsorption Using *In Situ* ATR-IR Spectroscopy

Shota Matsuo and Atsushi Urakawa*

Cite This: *Langmuir* 2025, 41, 33586–33593
Read Online



**ABSTRACT:** Single-atom catalysts, which consist of isolated metal sites immobilized on the support, have attracted significant attention in heterogeneous catalysis due to their high catalytic performance. The so-called strong electrostatic adsorption (SEA), in which a metal precursor is deposited onto an oxide support by electrostatic attraction, is widely employed to obtain single-atom catalysts in wet synthesis. In this work, we investigated the adsorption behavior of Re precursor, perrhenate, on anatase titania as an example of SEA studied by *in situ* attenuated total reflection infrared (ATR-IR) spectroscopy. The study confirms that the adsorption of perrhenate on titania is enhanced at a lower pH, which is consistent with a SEA model, and that the adsorption and desorption processes are reversible at pH 3.0. The ATR-IR spectroscopic kinetic analysis of the adsorption processes of perrhenate in nitric acid, assuming the Langmuir adsorption model, reveals that the kinetics of the perrhenate adsorption onto titania is influenced by the ionic strength. Furthermore, the adsorption mechanism of perrhenate changes depending on pH between 3.0 and 5.0. This study demonstrates that *in situ* ATR-IR spectroscopy is a powerful tool for the real-time monitoring and the kinetic study of SEA processes to design atomically engineered catalytic active sites.

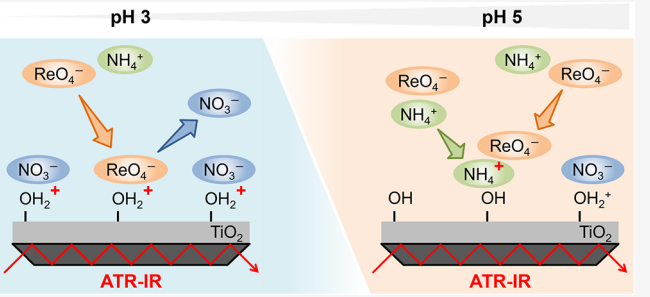




## INTRODUCTION

Supported metal catalysts have been extensively employed to produce valuable chemicals in industry.[1−3] Reducing the size of metal particles on the support is a general strategy to achieve the high surface-to-volume ratio for high atomic efficiency and to increase the population of low-coordination sites which are expected to exhibit high catalytic activity, while controlling the particle shape modulates the facets exposed on the surface.[4] In this context, single-atom catalysts (SACs), which typically consist of isolated metal sites immobilized on the support, are the ultimate small-size limit of metal catalysts with the maximum atom utilization efficiency, unsaturated coordination configurations, and site homogeneity.[5,6] SACs have shown remarkable catalytic performance in thermocatalysis,[7,8] electrocatalysis,[9] and photocatalysis,[10] and thus have gained considerable attention in the catalysis community.

Although constructing single metal atoms on the support by lowering the metal loading is relatively easy at the expense of catalytic activity, it is still challenging to fabricate SACs at high metal loading and avoid the aggregation of the single metal atoms because their surface energy is higher than that of the corresponding metal clusters and nanoparticles.[11] From this point of view, the stabilization of isolated atoms on the support is a vital issue in the design and synthesis of SACs. Strong electrostatic adsorption (SEA), in which a metal precursor is deposited onto the oxide support by electrostatic attraction, is one of the conventional methods[12] to obtain SACs in wet synthesis.[13−15] The surface of oxides such as $TiO_2$, $Al_2O_3$, and $SiO_2$ is positively charged by the protonation of the surface hydroxyl groups of the support in aqueous solutions at lower pH than the point of zero charge (PZC) of the support or negatively charged by the deprotonation at higher pH than the support PZC. This physical property of oxides allows an anionic or cationic metal precursor to be electrostatically adsorbed in aqueous solutions onto the oxide support charged positively or negatively, respectively, in the process of SEA. The undesired ligands covering the metal atoms can be removed by post-treatment.[16]

Since the SEA method highly relies upon the electrostatic adsorption behavior of metal precursors on oxide supports to achieve atomic dispersion on the support surface, understanding and controlling the adsorption behavior are of fundamental importance to synthesize desired SACs by this

Received: October 5, 2025
Revised: November 17, 2025
Accepted: November 18, 2025
Published: December 3, 2025





https://doi.org/10.1021/acs.langmuir.5c05228
*Langmuir* 2025, 41, 33586−33593

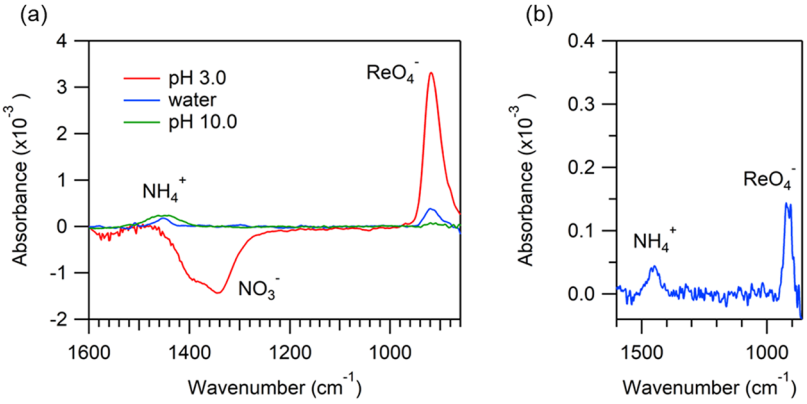


**Figure 1.** (a) ATR-IR spectra measured using titania films on a germanium IRE under the flow of 0.5 mM ammonium perrhenate solutions of pH 3.0 nitric acid (red), water (blue), and pH 10.0 aqueous ammonium (green). The flow rate was 0.8 mL $min^{-1}$. These spectra were obtained by averaging three cycles (250 × 3 scans). (b) ATR-IR spectrum of 0.5 mM ammonium perrhenate in pH 3.0 nitric acid on a bare germanium IRE.

method. It is pointed out that pH values of aqueous solutions can be shifted during the SEA process, and consequently, the quality of resulting SACs is affected.[17] The adsorption behavior of metal precursors is also affected by the heterogeneity of the functional groups and the presence of defects on the surface of the oxide support. To date, the methodologies for the determination of PZC values for oxides[18] and the quantification of metal precursor uptake on oxides as a function of pH and metal concentration using inductively coupled plasma spectroscopy[13,19,20] have been well established. Quartz crystal microbalance was applied for the *in situ* monitoring of the interaction between metal complexes and oxide surfaces at liquid−solid interface.[21,22] *In situ* resonant anomalous X-ray reflectivity revealed the geometric structure and spectroscopic properties of $Pt(NH_3)_4^{2+}$ adsorbed at the quartz(100)-water interface.[23] In addition, it is reported that metal uptake on a support can be predicted *via* the revised physical adsorption model.[24,25] Nevertheless, although the liquid phase in the SEA system typically contains an ionic metal precursor as well as its counterion, acid, base, and solvent, the real-time monitoring of the adsorption behavior has not yet been explored with distinguishing each chemical species in the system.

Attenuated total reflection infrared (ATR-IR) spectroscopy is a powerful technique to investigate the adsorption behavior at the liquid−solid interface at the molecular level under *in situ* conditions.[26,27] In this technique, a thin film of a solid adsorbent is deposited onto an internal reflection element (IRE) and immersed in the liquid phase containing adsorbates. Incident infrared light travels through the IRE and undergoes total reflection at the surface of the IRE. The evanescent waves generated at the reflection interface interact with the surrounding molecules, allowing one to monitor the molecular vibrations at the liquid−solid interface. The penetration depth of the evanescent waves into the liquid phase reaches only a few hundred nanometers to a few micrometers, which helps sensitive detection of the adsorbed molecules by minimizing the infrared absorption of the liquid phase. Moreover, ATR-IR spectroscopy has been applied to study the dynamic interfacial processes due to its good time resolution.[28−31]

In this work, we investigate the adsorption behavior of perrhenate on anatase titania as the process to prepare $Re/TiO_2$[32] as an exemplifying case of SEA[33] by *in situ* ATR-IR spectroscopy using a multireflection germanium IRE coated with anatase titania. We first monitored the SEA processes using acidic, neutral, and basic media by *in situ* ATR-IR spectroscopy. Then, we performed the ATR-IR spectroscopic kinetic analysis at different pHs in the acidic range assuming the Langmuir adsorption model.

## EXPERIMENTAL SECTION

Anatase titania powder (ST-01, particle size of 7 nm and specific surface area of 300 $m^2/g$) was supplied by Ishihara Sangyo. Isopropanol and nitric acid were supplied by Honeywell. Ammonium hydroxide solution and ammonium perrhenate were supplied by Sigma-Aldrich. All the analytical reagents were used as received. Germanium trapezoid IRE (80 × 10 × 4 $mm^3$, 45°, 10 reflections) for ATR-IR spectroscopy was purchased from Knight Optical. Milli-Q water (18.2 MΩ·cm at 25 °C) was used throughout the experiments.

ATR-IR measurements were performed on a Vertex 70 FT-IR spectrometer (Bruker) equipped with a liquid-nitrogen-cooled MCT detector and a horizontal attenuated total reflectance (HATR) accessory (Pike Technologies). The multireflection germanium IRE was fixed within the HATR cell and sealed with Viton O-rings. The cell volume was approximately 1 mL. Anatase titania was deposited on the IRE mounted in the cell using 400 μL of the suspension of titania in isopropanol (7.5 mg $mL^{-1}$). The thickness of the deposited titania layer is estimated to be around 1.4 μm based on the amount of $TiO_2$ added. The suspension was dried on the IRE in the air at room temperature. Water was passed through the cell for 2 h using a peristaltic pump (BT100L, Golander) to remove loosely attached titania from the IRE. Then, the water was displaced with an aqueous solution with pH adjusted by a pH meter (sensION+ PH3, HACH) and a background IR spectrum was collected for 500 scans. After the background collection, an aqueous perrhenate solution at the same pH was provided to the cell to study the adsorption of perrhenate on titania. IR spectra were acquired at a spectral resolution of 4 $cm^{-1}$ with 250 and 20 scans for low (0.8 mL $min^{-1}$) and high (20 mL $min^{-1}$) flow rates, respectively. It took approximately 9 s for 20 scans. 0.5 mM ammonium perrhenate solutions of pH 3.0 nitric acid, water, and pH 10.0 aqueous ammonium were used for measurements at a flow rate of 0.8 mL $min^{-1}$, and 0.25, 0.5, 1.0 mM ammonium perrhenate solutions of pH 3.0, 4.0, 5.0 nitric acid were used for measurements at a flow rate of 20 mL $min^{-1}$. For the time-resolved measurements at pH 3.0, 4.0, and 5.0 at a flow rate of 20 mL $min^{-1}$, the same titania-coated IRE was repeatedly used in three measurements using 0.25, 0.5, and 1.0 mM ammonium perrhenate solutions at the same pH after rinsing with an aqueous solution with the adjusted pH until no spectral change appeared, and a new titania film was produced for every pH. All the measurements were conducted at room temperature. Typically, spectra were collected with an aperture size of 4 mm and a scan velocity of 20 kHz.


https://doi.org/10.1021/acs.langmuir.5c05228
Langmuir 2025, 41, 33586−33593

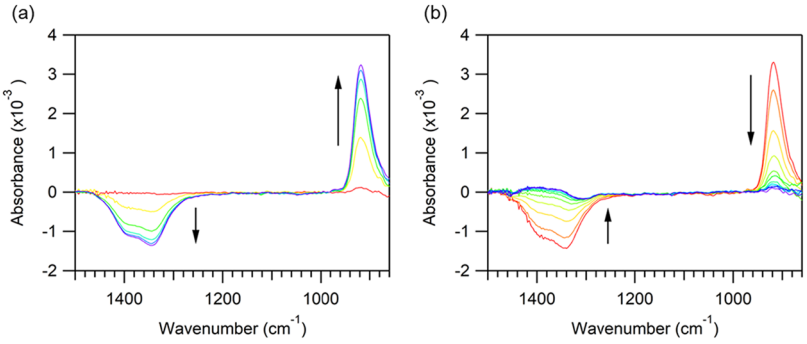


**Figure 2.** Time-resolved ATR-IR spectra measured using a titania film on a germanium IRE every 1.85 min (a) during the flow of 0.5 mM ammonium perrhenate solutions of pH 3.0 nitric acid and (b) the subsequent rinsing with pH 3.0 nitric acid. The flow rate was 0.8 mL min$^{-1}$.

## RESULTS AND DISCUSSION

Figure 1a shows the steady-state ATR-IR spectra measured using titania films coated on a germanium IRE under the flow of 0.5 mM ammonium perrhenate solutions of (i) pH 3.0 nitric acid, (ii) water, and (iii) pH 10.0 aqueous ammonium. The spectrum at pH 3.0 showed a positive peak at 918 cm$^{-1}$ and negative peaks at 1344 and 1390 cm$^{-1}$, which are assigned to $ReO_4^-$ stretching mode and $NO_3^-$ stretching modes, respectively.[34,35] It has been reported that the pristine titania, ST-01, does not show any absorption peaks at those frequencies.[36] The positive peak for perrhenate indicates the adsorption of perrhenate on titania, and the negative peak for nitrate indicates the desorption of nitrate. It should be noted that the absorbance of perrhenate in the liquid phase or adsorbed on the germanium IRE under these conditions was estimated to be at most ∼0.1 × 10$^{-3}$ and thus negligible (Figure 1b). In the spectrum for water, a positive perrhenate peak was observed, but the intensity was lower than that at pH 3.0, which suggests that the perrhenate adsorption was suppressed in water. The pH of 0.5 mM ammonium perrhenate in water was measured to be approximately 7, with a fluctuation in pH likely due to the influence of dissolved carbon dioxide in the solution. Since the PZC of the anatase titania used in this study (ST-01) is reported to be 6.3,[37] this result is consistent with the fact that the adsorption of perrhenate on titania relies on electrostatic interaction. Still, the absorbance reached ∼0.4 × 10$^{-3}$, indicating that the adsorption of perrhenate on titania occurred slightly. The peak position of perrhenate adsorbed in water showed no significant difference compared with that at pH 3.0. The positive peak due to ammonium was also observed at 1452 cm$^{-1}$.[38] The pristine titania shows no peak at this frequency.[36] At pH 10.0, the absorbance due to perrhenate decreased to ∼0.1 × 10$^{-3}$, which means that the perrhenate adsorption onto titania is negligible under the basic conditions.

To perform real-time monitoring of the progression of perrhenate adsorption and desorption, we measured time-resolved ATR-IR spectra during the adsorption process under the flow of 0.5 mM ammonium perrhenate solutions of pH 3.0 nitric acid and the subsequent rinsing process with pH 3.0 nitric acid (Figure 2). During both processes, no shift of the peak attributed to perrhenate at 918 cm$^{-1}$ was observed, which implies no significant change in the chemical state or lateral interactions of perrhenate adsorbed on titania under varying coverage. In Figure 2b, adsorbed perrhenate was removed to a negligible level by rinsing, indicating that the adsorption and desorption of perrhenate on titania at pH 3.0 are reversible processes. Finally, through the results shown in Figures 1 and 2, it has been demonstrated that *in situ* ATR-IR spectroscopy allows real-time monitoring of the amount and chemical state of each adsorbed species under various conditions of SEA processes.

Motivated by the results that the adsorption and desorption processes of perrhenate on titania are reversible under the acidic conditions and no significant change in the chemical state of adsorbed perrhenate occurs at varying amounts of adsorbates, we performed the kinetic analysis at pH 3.0, 4.0, and 5.0 using *in situ* ATR-IR spectroscopy assuming the Langmuir adsorption model. The revised physical adsorption model[24,25] also employs the Langmuir adsorption isotherm to describe the adsorption of metal ions onto oxide surfaces. We assume a reversible adsorption process of perrhenate on titania expressed as

$$ReO_4^- + V \underset{k_d}{\overset{k_a}{\rightleftarrows}} {ReO_4^-}_{ad} \tag{1}$$

where V and ${ReO_4^-}_{ad}$ are the vacant sites on titania surface and adsorbed perrhenate, respectively, and $k_a$ (M$^{-1}$ s$^{-1}$) and $k_d$ (s$^{-1}$) are the rate constants of the adsorption and desorption processes, respectively. Under a certain pH, the respective adsorption and desorption rates can be written as

$$r_a = k_a C(1 - \theta) \tag{2}$$

$$r_d = -k_d \theta \tag{3}$$

where $C$ (M$^{-1}$) and $\theta$ are the concentration of perrhenate and the surface coverage, respectively. Thus, the overall rate equation can be expressed as

$$\frac{\mathrm{d}}{\mathrm{d}t}\theta = r_a + r_d = k_a C(1 - \theta) - k_d \theta \tag{4}$$

where $t$ (s) is the sorption time. By integrating eq 4 with the boundary condition of $\theta = 0$ at $t = 0$ and with the assumption that $C$ is time-independent, we obtain

$$\theta = \frac{KC}{KC + 1}[1 - \mathrm{e}^{-k' t}] \tag{5}$$

$$K = \frac{k_a}{k_d} \tag{6}$$

$$k' = k_a C + k_d \tag{7}$$

where $K$ (M$^{-1}$) and $k'$ (s$^{-1}$) are the adsorption equilibrium constant and the apparent rate constant, respectively. $C$ can be seen as a time-independent constant if perrhenate is provided


https://doi.org/10.1021/acs.langmuir.5c05228
Langmuir 2025, 41, 33586−33593

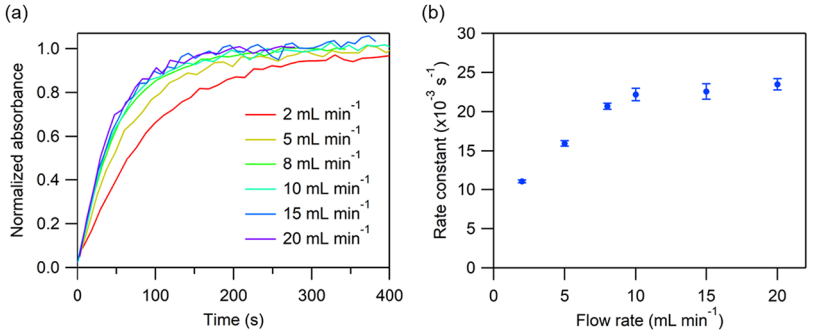


**Figure 3.** (a) Evolution of the normalized absorbance at 918 $cm^{-1}$ due to $ReO_4^-$ stretching as a function of time under the flow of 0.5 mM ammonium perrhenate solutions of pH 3.0 nitric acid at different flow rates. (b) Apparent rate constants of the time evolution as a function of flow rate obtained by curve fitting following eq 8.

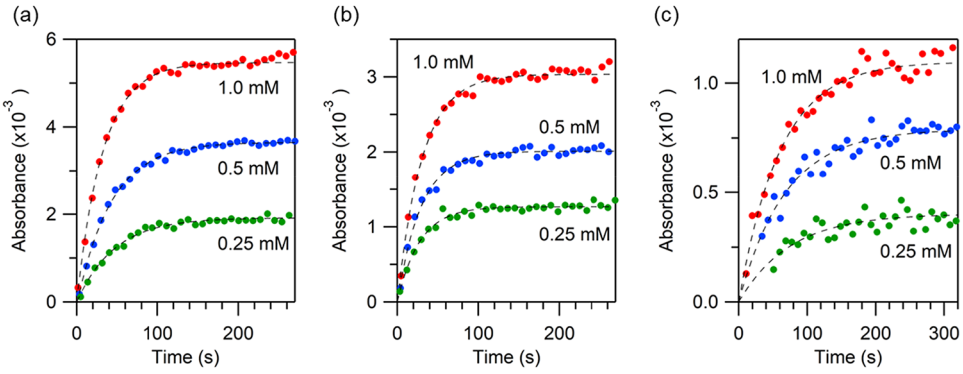


**Figure 4.** Time evolution of the absorbance at 918 $cm^{-1}$ under the flow of 0.25 (green), 0.5 (blue), and 1.0 (red) mM ammonium perrhenate solutions of (a) pH 3.0, (b) 4.0, and (c) 5.0 nitric acid. The flow rate was 20 mL $min^{-1}$. The dashed curves show the fitting results.

fast enough, that is, at a high enough flow rate. Since the ATR-IR absorbance at 918 $cm^{-1}$ due to adsorbed perrhenate, denoted as $A$, is proportional to the adsorbed amount and hence to $\theta$, $A$ can be expressed as

$$A = A_\infty[1 - e^{-k't}] \tag{8}$$

$$A_\infty = A_{sat} \cdot \frac{KC}{KC + 1} \tag{9}$$

where $A_\infty$ is the steady-state absorbance at 918 $cm^{-1}$ and $A_{sat}$ corresponds to the absorbance at 918 $cm^{-1}$ at saturated adsorption of perrhenate. Thus, $k'$ can be obtained by fitting the change of $A$ in time with eq 8 at a constant concentration of perrhenate. Assuming that $k_a$ and $k_d$ are independent of perrhenate concentration, the linear fitting of $k'$ for perrhenate concentration gives $k_a$ and $k_d$ based on eq 7. Furthermore, if $A_{sat}$ is independent of the perrhenate concentration, the curve fitting of $A_\infty$ for the perrhenate concentration based on eq 9 gives $K$ and $A_{sat}$.

As mentioned above, the flow rate of the perrhenate solution must be high enough that $C$ can be considered to be constant. We examined how the apparent rate constant, $k'$, depends on the flow rate. Figure 3a shows the evolution of the normalized absorbance at 918 $cm^{-1}$ due to $ReO_4^-$ stretching as a function of time under the flow of 0.5 mM ammonium perrhenate solutions of pH 3.0 nitric acid at different flow rates. There is a clear trend that the time taken for the normalized absorbance to reach its equilibrium value of 1 is shorter at higher flow rates. The $k'$ values obtained by fitting the data following eq 8 are shown in Figure 3b as a function of flow rate. At flow rates less than 10 mL $min^{-1}$, $k'$ is heavily dependent on the flow rate, indicating that the adsorption process was limited by external mass transfer.[39] In contrast, no significant change in $k'$ is observed at flow rates between 10 and 20 mL $min^{-1}$. Therefore, we set the flow rate at 20 mL $min^{-1}$ to minimize the mass transfer limitation in the present kinetic study.

We performed time-resolved ATR-IR measurements for the perrhenate adsorption on titania under the flow of 0.25, 0.5, and 1.0 mM ammonium perrhenate solutions of pH 3.0, 4.0, and 5.0 nitric acid (Figure 4). These pH values are lower than the reported PZC value of 6.3 for the anatase titania (ST-01).[37] First, there is an increasing trend for the amounts of adsorbates at steady-state at lower pH. This would be largely attributed to the higher degree of protonation of the titania surface at lower pH, which promotes the electrostatic attraction between titania and perrhenate. In addition, all the obtained results were well fit with eq 8, which confirms that the Langmuir adsorption model is valid in these systems. The $k'$ values obtained by this fitting analysis clearly depend on pH, as shown in Figure 5. These results illustrate that pH affects not only the concentration of the adsorbates but also the kinetics of perrhenate adsorption during SEA processes.

In the case of pH 3.0, $k'$ changed linearly with perrhenate concentration and the linear fitting of $k'$ gave $k_a$ = 12.6 ± 1.3 $M^{-1}$ $s^{-1}$ and $k_d$ = 0.018 ± 0.001 $s^{-1}$, thus $k_a/k_d$ = 704 ± 81 $M^{-1}$. In addition, the steady-state absorbance at 918 $cm^{-1}$ was well fit for perrhenate concentration following eq 9 (Figure 6a), which yielded $K$ = 753 ± 19 $M^{-1}$ and $A_{sat}$ = 0.0129 ± 0.0002. This $K$ value is in good agreement with the obtained values of $k_a/k_d$, as expected in eq 6. These results imply that $k_a$ and $k_d$ do not depend significantly on perrhenate concentration in the range of 0.25 to 1.0 mM at pH 3.0.


https://doi.org/10.1021/acs.langmuir.5c05228
Langmuir 2025, 41, 33586−33593

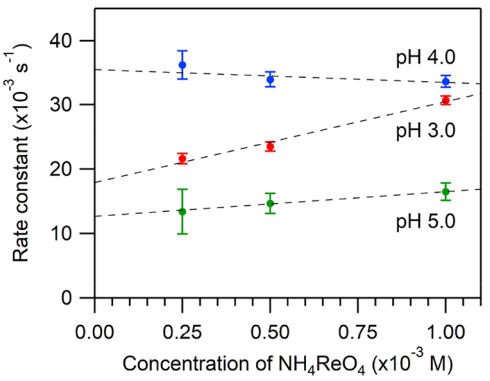


**Figure 5.** Apparent rate constants, $k'$, as functions of perrhenate concentration at pH 3.0 (red), 4.0 (blue), and 5.0 (green). The dashed lines show the linear approximation.

For pH 4.0, the linear fitting of $k'$ gave $k_a = -2.0 \pm 2.5$ M$^{-1}$ s$^{-1}$ and $k_d = 0.036 \pm 0.002$ s$^{-1}$, thus $k_a/k_d = -56 \pm 70$ M$^{-1}$. However, the curve fitting of the steady-state absorbance at 918 cm$^{-1}$ yielded $K = 1011 \pm 29$ M$^{-1}$ on the basis of eq 9 (Figure 6b), which is inconsistent with the obtained $k_a/k_d$. The $A_{sat}$ value obtained was 0.0059 ± 0.0001, which was smaller than that for pH 3.0. This likely reflects the lower number of protonated adsorption sites on titania at pH 4.0 than at pH 3.0. Also, for pH 5.0 in a similar manner, $k_a/k_d$ was estimated to be 299 ± 283 M$^{-1}$ ($k_a = 3.8 \pm 3.5$ M$^{-1}$ s$^{-1}$, $k_d = 0.013 \pm 0.003$ s$^{-1}$), while $K$ was obtained as 940 ± 88 M$^{-1}$ ($A_{sat} = 0.0024 \pm 0.0001$), as shown in Figure 6c.

These discrepancies indicate that the estimation of $k_a$, $k_d$, and $K$ according to eqs 7 and 9 was not appropriate at pH 4.0 and 5.0. As the fitting analysis following eqs 7 and 9 is employed assuming that $k_a$, $k_d$, and $K$ and $A_{sat}$ are independent of perrhenate concentration, it is likely that the discrepancies were caused by the dependence of those constants on perrhenate concentration. The revised physical adsorption model[25] describes that metal uptake onto supports decreases at high ionic strength. In the present study, the concentrations of nitric acid in the aqueous solutions at pH 4.0 and 5.0 (0.1 and 0.01 mM, respectively) are lower than those of ammonium perrhenate (0.25, 0.5, and 1.0 mM). Hence, the ionic strength in these aqueous solutions is highly dependent on the perrhenate concentration. The higher ionic strength weakens the electrostatic attraction between perrhenate and titania surface, as previously reported using other precursors.[25,40,41] Consequently, $K$, or $k_a/k_d$, will decrease with an increasing perrhenate concentration at pH 4.0 and 5.0. Besides, the extent of protonation of titania increases with the increasing ionic strength in aqueous solutions,[42] which means that $A_{sat}$ can also depend on the perrhenate concentration. On the other hand, the agreement between the obtained values of $k_a/k_d$ and $K$ for pH 3.0 can be described by the fact that the nitric acid concentration at pH 3.0 is 1 mM and is therefore higher than or comparable to the ammonium perrhenate concentrations used in the present measurements. Therefore, we confirm that the ionic strength affects the kinetic properties of the SEA processes.

In order to gain insight into the chemical species involved in the perrhenate adsorption at each pH, we examined the steady-state ATR-IR spectra of the interface between titania and 1 mM ammonium perrhenate in nitric acid at pH 3.0, 4.0, and 5.0 (Figure 7a–c). The peaks due to $ReO_4^-$ stretching were observed at 918 cm$^{-1}$ at all three pH values. The negative peaks due to nitrate were found at 1346 cm$^{-1}$ at pH 3.0 and 4.0, but no nitrate peak was detected at pH 5.0. The peaks due to ammonium were observed at 1456 cm$^{-1}$ at pH 4.0 and 5.0 with a similar absorbance of approximately $0.25 \times 10^{-3}$. Since the contribution of ammonium in the liquid phase of 1 mM ammonium perrhenate can be estimated to be at most ~$0.1 \times 10^{-3}$ in absorbance according to the result shown in Figure 1b, the result confirms that ammonium was adsorbed on titania from 1 mM ammonium perrhenate in nitric acid at pH 4.0 and 5.0. No peak due to ammonium was detected at pH 3.0, which might be because it overlaps with the large negative peak of nitrate.

Moreover, the changes over time in absorbance of perrhenate, nitrate, and ammonium for each pH after ammonium perrhenate injection were compared in Figure 7d–f. To obtain apparent rate constants, $k'$, fitting analysis was performed for all the results by applying a similar equation to eq 8 based on the Langmuir adsorption model. The uncertainties in the rate constants were obtained by fitting analysis. At pH 3.0, the adsorption of perrhenate and the desorption of nitrate were synchronized, as evidenced by the good agreement in the apparent rate constants for the adsorption and desorption. Apparently, this shows that the anion exchange between nitrate and perrhenate occurred at the titania surface during the perrhenate adsorption process (Figure 8a). Both of the anions are likely to be adsorbed on the protonated titania surface due to electrostatic attraction.

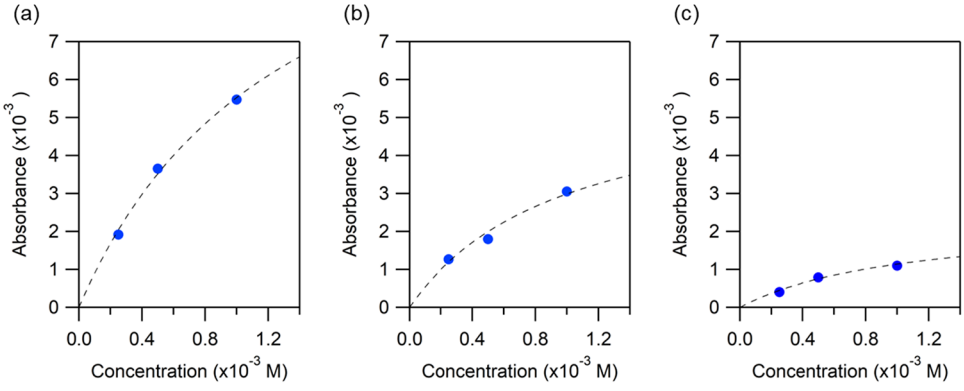


**Figure 6.** Steady-state absorbance at 918 cm$^{-1}$ as a function of perrhenate concentration in (a) pH 3.0, (b) pH 4.0, and (c) pH 5.0 nitric acid. The dashed curves show the best fitting results following eq 9.


https://doi.org/10.1021/acs.langmuir.5c05228
Langmuir 2025, 41, 33586–33593

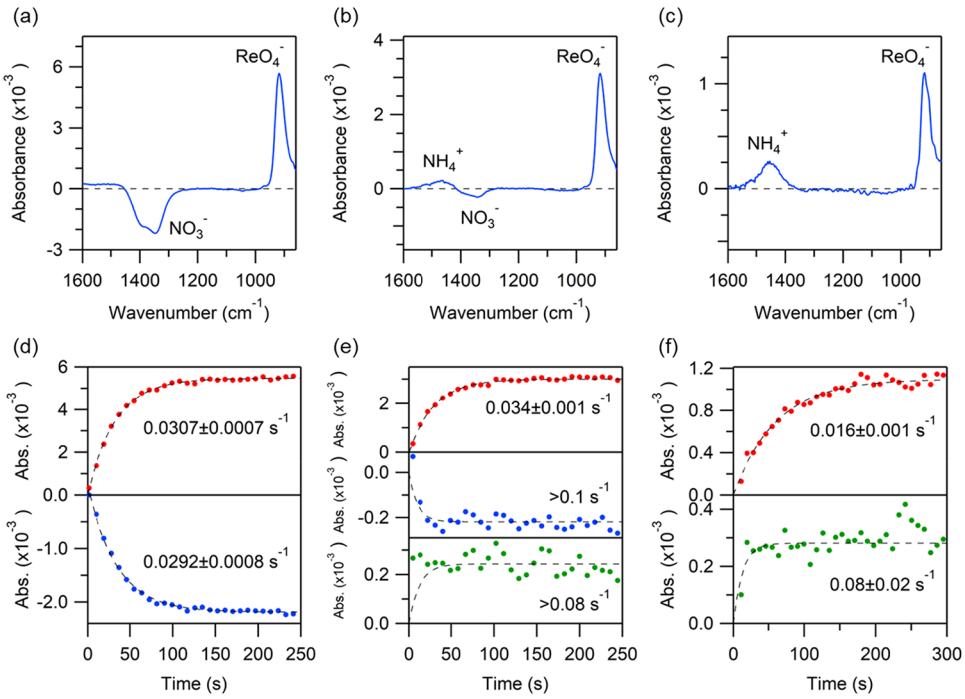


**Figure 7.** (a–c) Steady-state ATR-IR spectra under the flow of 1.0 mM ammonium perrhenate solutions of (a) pH 3.0, (b) 4.0, and (c) 5.0 nitric acid using titania films on a germanium IRE. These spectra were obtained by averaging ten cycles (20 × 10 scans). (d–f) Time evolution of the absorbance at 918 $cm^{-1}$ for perrhenate (red), 1346 $cm^{-1}$ for nitrate (blue), and 1456 $cm^{-1}$ for ammonium (green) under the flow of 1.0 mM ammonium perrhenate solutions of (d) pH 3.0, (e) 4.0, and (f) 5.0 nitric acid. The dashed curves show the fitting results based on the Langmuir adsorption model. The values in the figures indicate apparent rate constants.

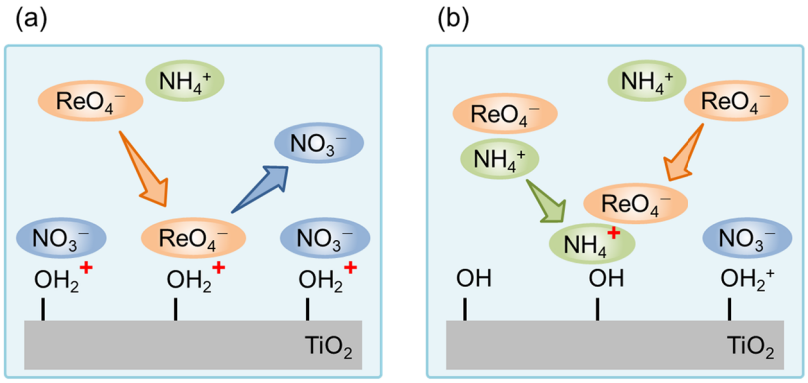


**Figure 8.** Two proposed mechanisms governing the perrhenate adsorption on titania from aqueous nitric acid solutions. (a) Anion exchange between nitrate and perrhenate. (b) Perrhenate adsorption onto titania surface charged positively by preadsorbed ammonium.

The absorbance at 1346 $cm^{-1}$ due to adsorption on titania in pH 3.0 nitric acid is ~4 × $10^{-3}$ (Figure S2), while the nitrate absorbance decreased by ~2 × $10^{-3}$ upon the perrhenate adsorption. This indicates that approximately half of the nitrate adsorbed on titania was replaced with perrhenate. In contrast, at pH 4.0, the nitrate desorption was faster than the perrhenate adsorption, which means that the perrhenate adsorption was governed by not only anion exchange but also other mechanisms. It should be noted that, in the case for pH 4.0, the first and second spectra (at 5 and 13 s, respectively) after switching to 1 mM ammonium perrhenate at pH 4.0 was distorted between 1300 and 1600 $cm^{-1}$, which affected the absorbance at the peak position for nitrate. From the third spectrum onward (at 22 s), the spectral change in the region of the nitrate peak was small, which means that the nitrate desorption reached its equilibrium within 22 s. Given that the uncertainty of the absorbance of nitrate at its equilibrium is 12%, we estimated the apparent rate constant for nitrate to be >0.1 $s^{-1}$ by assuming that 88% of the absorbance at the equilibrium for nitrate are reached within 22 s. As shown in Figure 7a,b, the negative peak intensity of nitrate relative to the positive peak intensity of perrhenate at pH 4.0 is smaller than that at pH 3.0. This supports the smaller contribution of the anion exchange in the perrhenate adsorption on titania at pH 4.0. In the case of pH 4.0, the absorbance at 1346 $cm^{-1}$ of adsorbed nitrate is ~0.8 × $10^{-3}$, as shown in Figure S2, while the nitrate absorbance decreased by ~0.2 × $10^{-3}$ upon the perrhenate adsorption. In addition, since no clear nitrate peak was detected at pH 5.0 in Figure 7c, the perrhenate adsorption at pH 5.0 is hardly controlled by the anion exchange between nitrate and perrhenate.


https://doi.org/10.1021/acs.langmuir.5c05228
Langmuir 2025, 41, 33586–33593

At pH 4.0 and 5.0, the apparent rate constants of ammonium were found to be higher than those of perrhenate (Figure 7e,f). In the case for pH 4.0, considering the spectral distortion mentioned above, we estimated the apparent rate constant for ammonium to be >0.08 $s^{-1}$ with the uncertainty of 17% in its equilibrium absorbance. Given that the adsorption of ammonium cations on titania gives positive charges on the surface, this result suggests that ammonium was quickly adsorbed onto titania to make the surface charge positively followed by the electrostatic adsorption of perrhenate onto the titania surface at pH 4.0 and 5.0 (Figure 8b). Perrhenate can be interpreted as being adsorbed to adjust the charge balance instead of nitrate. This adsorption mechanism does not require the protonation of titania surface as contrasted to the anion exchange mechanism. The peak intensity of ammonium relative to that of perrhenate is increased at higher pH, as shown in Figure 7a−c, which suggests that the perrhenate adsorption onto the titania surface positively charged by preadsorbed ammonium was more pronounced at higher pH. This trend is the opposite of the case of the anion exchange between nitrate and perrhenate. This would be because the higher degree of protonation of titania at lower pH enhances the electrostatic adsorption of anions and the electrostatic repulsion between ammonium and the protonated titania surface. We conclude that the contributions of these two mechanisms to the perrhenate adsorption on titania from aqueous nitric acid solutions depend on pH, and hence the adsorption kinetic properties of perrhenate onto titania vary with pH as shown in Figure 5.

Our present ATR-IR spectroscopic results elucidate that the kinetic properties of the SEA of perrhenate onto titania are influenced by pH and ionic strength, and the adsorption mechanism of perrhenate changes depending on pH. Since the quality of single-atom catalysts synthesized by SEA methods is affected by pH values of aqueous solutions during synthesis,[17] understanding the underlying mechanism for the pH effects is crucial to obtain improved catalysts. By combination with further investigations on the structure of resulting catalysts, the present findings will help to understand how synthetic conditions such as pH and ionic strength govern the structural evolution during synthesis, consequently contributing to the design of atomically engineered catalytic active sites. Also, the data concerning the kinetics and mechanism of SEA processes demonstrated in this study can only be obtained by analytical techniques that have good time resolution and distinguish chemical species. Hence, the present approach using *in situ* ATR-IR spectroscopy provides unique insights into the kinetics and mechanisms of SEA processes.

## CONCLUSIONS

We have investigated the adsorption behavior of perrhenate onto anatase titania from aqueous solutions at different pH values by *in situ* ATR-IR spectroscopy. The measurements under acidic, neutral, and basic conditions confirmed that the adsorption amount of perrhenate is increased at a lower pH from the absorbance change. The ATR-IR spectroscopic kinetic study of the perrhenate adsorption from aqueous nitric acid solutions based on the Langmuir adsorption model showed that the kinetic properties of perrhenate adsorption are affected by ionic strength. Also, the perrhenate adsorption on titania is governed by the anion exchange between nitrate and perrhenate at pH 3.0, while the adsorption onto the titania surface positively charged by preadsorbed ammonium is more dominant at pH 5.0. Through the present study, we have demonstrated that *in situ* ATR-IR spectroscopy allows the real-time monitoring and the kinetic study of SEA processes by distinguishing each chemical species to design atomically engineered catalytic active sites.

## ASSOCIATED CONTENT

### Supporting Information

The Supporting Information is available free of charge at https://pubs.acs.org/doi/10.1021/acs.langmuir.5c05228.

X-ray diffraction pattern of anatase titania used in this study; ATR-IR spectra of nitrate adsorbed on titania films; and time-resolved ATR-IR spectra measured under the flow of 1.0 mM ammonium perrhenate solutions on a titania film (PDF)

## AUTHOR INFORMATION


### Corresponding Author

**Atsushi Urakawa** − *Catalysis Engineering, Department of Chemical Engineering, Delft University of Technology, 2629 HZ Delft, Netherlands;* orcid.org/0000-0001-7778-4008; Email: A.Urakawa@tudelft.nl

### Author

**Shota Matsuo** − *Catalysis Engineering, Department of Chemical Engineering, Delft University of Technology, 2629 HZ Delft, Netherlands*

Complete contact information is available at: https://pubs.acs.org/10.1021/acs.langmuir.5c05228


### Author Contributions

The manuscript was written through contributions of all authors. All authors have given approval to the final version of the manuscript. S.M.: Conceptualization, methodology, validation, investigation, formal analysis, writing—original draft, visualization. A.U.: Conceptualization, methodology, supervision, writing—review and editing.

### Notes

The authors declare no competing financial interest.

## ACKNOWLEDGMENTS

The authors would like to acknowledge the inspiration drawn from the work of Dr. Benjamin Mockenhaupt (University of Duisburg-Essen).

## REFERENCES


(1) Stark, W. J.; Stoessel, P. R.; Wohlleben, W.; Hafner, A. Industrial Applications of Nanoparticles. *Chem. Soc. Rev.* **2015**, *44*, 5793−5805.

(2) Li, T.; Jia, D.; Zhou, S.; Liu, Z.; Chen, J.; Ban, T.; Li, A.; Li, H.; Gao, H. Review on recent advances in supported metal catalysts for synthesis of high energy density fuels. *Fuel* **2024**, *373*, No. 132329.

(3) Chu, M.; Kang, Q.; Hu, P.; Zhang, Q.; Chen, J. Unlocking opportunities: Supported metal catalysts for the chemical upcycling of waste plastics. *Chem. Eng. J.* **2024**, *496*, No. 154375.

(4) Xie, S. F.; Choi, S.; Xia, X. B.; Xia, Y. N. Catalysis on faceted noble-metal nanocrystals: both shape and size matter. *Curr. Opin. Chem. Eng.* **2013**, *2*, 142−150.

(5) Qiao, B.; Wang, A.; Yang, X.; Allard, L. F.; Jiang, Z.; Cui, Y.; Liu, J.; Li, J.; Zhang, T. Single-atom catalysis of CO oxidation using $Pt_1/FeO_x$. *Nat. Chem.* **2011**, *3*, 634−641.

(6) Chen, R.; Chen, S.; Wang, L.; Wang, D. Nanoscale metal particle modified single-atom catalyst: synthesis, characterization, and application. *Adv. Mater.* **2024**, *36*, No. 2304713.

(7) Zhang, H.; Liu, G.; Shi, L.; Ye, J. Single-Atom Catalysts: Emerging Multifunctional Materials in Heterogeneous Catalysis. *Adv. Energy Mater.* **2018**, *8*, No. 1701343.
(8) Guo, W.; Wang, Z.; Wang, X.; Wu, Y. General Design Concept for Single-Atom Catalysts toward Heterogeneous Catalysis. *Adv. Mater.* **2021**, *33*, No. e2004287.
(9) Humayun, M.; Israr, M.; Khan, A.; Bououdina, M. State-of-the-art single-atom catalysts in electrocatalysis: from fundamentals to applications. *Nano Energy* **2023**, *113*, No. 108570.
(10) Wei, T.; Zhou, J.; An, X. Recent advances in single-atom catalysts (SACs) for photocatalytic applications. *Mater. Rep.: Energy* **2024**, *4*, No. 100285.
(11) Weon, S.; Huang, D.; Rigby, K.; Chu, C.; Wu, X.; Kim, J.-H. Environmental materials beyond and below the nanoscale: Single-atom catalysts. *ACS EST Eng.* **2021**, *1*, 157−172.
(12) Loy, A. C. M.; Teng, S. Y.; How, B. S.; Zhang, X.; Cheah, K. W.; Butera, V.; Leong, W. D.; Chin, B. L. F.; Yiin, C. L.; Taylor, M. J.; Kyriakou, G. Elucidation of single atom catalysts for energy and sustainable chemical production: Synthesis, characterization and frontier science. *Prog. Energy Combust. Sci.* **2023**, *96*, No. 101074.
(13) Schreier, M. A Fundamental Study of Pt Tetraammine Impregnation of Silica: 1. The Electrostatic Nature of Platinum Adsorption. *J. Catal.* **2004**, *225*, 190−202.
(14) Bo, Z.; McCullough, L. R.; Dull, S.; Ardagh, M. A.; Wang, J.; Notestein, J. Strong Electrostatic Adsorption of Pt onto $SiO_2$ Partially Overcoated $Al_2O_3$—Towards Single Atom Catalysts. *J. Chem. Phys.* **2019**, *151*, No. 214703.
(15) Wang, Y.; Qin, S.; Denisov, N.; Kim, H.; Bad'ura, Z.; Sarma, B. B.; Schmuki, P. Reactive Deposition Versus Strong Electrostatic Adsorption (SEA): A Key to Highly Active Single Atom Co-Catalysts in Photocatalytic $H_2$ Generation. *Adv. Mater.* **2023**, *35*, No. 2211814.
(16) Li, R.; Luo, L.; Ma, X.; Wu, W.; Wang, M.; Zeng, J. Single Atoms Supported on Metal Oxides for Energy Catalysis. *J. Mater. Chem. A* **2022**, *10*, 5717−5742.
(17) Guo, J.; Liu, H.; Li, D.; Wang, J.; Djitcheu, X.; He, D.; Zhang, Q. A minireview on the synthesis of single atom catalysts. *RSC Adv.* **2022**, *12*, 9373−9394.
(18) Bourikas, K.; Kordulis, C.; Lycourghiotis, A. Titanium dioxide (anatase and rutile): Surface chemistry, liquid−solid interface chemistry, and scientific synthesis of supported catalysts. *Chem. Rev.* **2014**, *114*, 9754−9823.
(19) Jiao, L.; Regalbuto, J. R. The synthesis of highly dispersed noble and base metals on silica via strong electrostatic adsorption: I. Amorphous silica. *J. Catal.* **2008**, *260*, 329−341.
(20) Wong, A.; Liu, Q.; Griffin, S.; Nicholls, A.; Regalbuto, J. R. Synthesis of Ultrasmall, Homogeneously Alloyed, Bimetallic Nanoparticles on Silica Supports. *Science* **2017**, *358*, 1427−1430.
(21) Hervier, A.; Blanchard, J.; Costentin, G.; Regalbuto, J.; Louis, C.; Boujday, S. The genesis of a heterogeneous catalyst: in situ observation of a transition metal complex adsorbing onto an oxide surface in solution. *Chem. Commun.* **2014**, *50*, 2409−2411.
(22) Blanchard, J.; Hervier, A.; Costentin, G.; Regalbuto, J.; Louis, C.; Boujday, S. *In-situ* monitoring of transition metal complex adsorption on oxide surfaces during the first stages of supported metal catalyst preparation. *Catal. Today* **2014**, *235*, 245−249.
(23) Park, C.; Fenter, P.; Sturchio, N.; Regalbuto, J. Probing Outer-Sphere Adsorption of Aqueous Metal Complexes at the Oxide-Water Interface with Resonant Anomalous X-Ray Reflectivity. *Phys. Rev. Lett.* **2005**, *94*, No. 076104.
(24) Agashe, K. B.; Regalbuto, J. R. A Revised Physical Theory for Adsorption of Metal Complexes at Oxide Surfaces. *J. Colloid Interface Sci.* **1997**, *185*, 174−189.
(25) Hao, X.; Spieker, W. A.; Regalbuto, J. R. A further simplification of the revised physical adsorption (RPA) model. *J. Colloid Interface Sci.* **2003**, *267*, 259−264.
(26) Hind, A. R.; Bhargava, S. K.; McKinnon, A. At the solid/liquid interface: FTIR/ATR — the tool of choice. *Adv. Colloid Interface Sci.* **2001**, *93*, 91−114.
(27) Andanson, J.-M.; Baiker, A. Exploring catalytic solid/liquid interfaces by in situ attenuated total reflection infrared spectroscopy. *Chem. Soc. Rev.* **2010**, *39*, 4571−4584.
(28) Ferri, D.; Bürgi, T.; Baiker, A. Probing Boundary Sites on a Pt/$Al_2O_3$ Model Catalyst by $CO_2$ Hydrogenation and In Situ ATR-IR Spectroscopy of Catalytic Solid-Liquid Interfaces. *Phys. Chem. Chem. Phys.* **2002**, *4*, 2667−2672.
(29) Urakawa, A.; Wirz, R.; Burgi, T.; Baiker, A. ATR-IR Flow-Through Cell for Concentration Modulation Excitation Spectroscopy: Diffusion Experiments and Simulations. *J. Phys. Chem. B* **2003**, *107*, 13061−13068.
(30) Ebbesen, S. D.; Mojet, B. L.; Lefferts, L. In situ ATR-IR study of nitrite hydrogenation over Pd/$Al_2O_3$. *J. Catal.* **2008**, *256*, 15−23.
(31) da Silva, M. J. E.; Banerjee, A.; Lefferts, L.; Albanese, J. A. F. In-situ ATR-IR Spectroscopy Reveals Complex Absorption-Diffusion Dynamics in Model Polymer-Membrane-Catalyst Assemblies (PCMA). *ChemCatChem* **2022**, *14*, No. 202101835.
(32) Phongprueksathat, N.; Ting, K. W.; Mine, S.; Jing, Y.; Toyoshima, R.; Kondoh, H.; Shimizu, K.-i.; Toyao, T.; Urakawa, A. Bifunctionality of Re Supported on $TiO_2$ in Driving Methanol Formation in Low-Temperature $CO_2$ Hydrogenation. *ACS Catal.* **2023**, *13*, 10734−10750.
(33) Yang, B.; Wang, Y.; Gao, B.; Zhang, L.; Guo, L. Size-Dependent Active Site and Its Catalytic Mechanism for $CO_2$ Hydrogenation Reactivity and Selectivity over Re/$TiO_2$. *ACS Catal.* **2023**, *13*, 10364−10374.
(34) Li, M.-M.; Cao, J.-W.; Qin, X.-L.; Liu, X.-Y.; Yuan, X.-Q.; Dong, X.-T.; Guo, Q.; Sun, Y.; Zhang, P. Theoretical Prediction of Rhenium Separation from Ammonium Perrhenate by Phonon-Photon Resonance Absorption. *ACS Omega* **2022**, *7*, 5437−5441.
(35) Baumgartner, B.; Freitag, S.; Gasser, C.; Lendl, B. A. Pocket-Sized 3D-printed Attenuated Total Reflection-Infrared Filtometer combined with Functionalized Silica Films for Nitrate Sensing in Water. *Sens. Actuators, B* **2020**, *310*, No. 127847.
(36) Aoyagi, M.; Funaoka, M. A new polymeric photosensitizer for dye-sensitized solar cell with porous $TiO_2$ from forest carbon resources. *J. Photochem. Photobiol., A* **2004**, *164*, 53−60.
(37) Zhang, J.; Nosaka, Y. Mechanism of the OH Radical Generation in Photocatalysis with $TiO_2$ of Different Crystalline Types. *J. Phys. Chem. C* **2014**, *118*, 10824−10832.
(38) Gonzalez-Rodriguez, J.; Pepper, K.; Baron, M. G.; Mamo, S. K.; Simons, A. M. Production and Analysis of Recycled Ammonium Perrhenate from CMSX-4 Superalloys. *Open Chem.* **2018**, *16*, 1298−1306.
(39) Amiri, H.; Ayati, B.; Ganjidoust, H. Mass transfer phenomenon in photocatalytic cascade disc reactor: Effects of artificial roughness and flow rate. *Chem. Eng. Process.* **2017**, *116*, 48−59.
(40) Eskandari, S.; Dong, A. H.; De Castro, L. T.; et al. Pushing the limits of electrostatic adsorption: charge enhanced dry impregnation of SBA-15. *Catal. Today* **2019**, *338*, 60−71.
(41) Kreatananchai, B.; Somsook, E.; Kiatsiriroat, T.; Punyawudho, K. Preparation of palladium catalysts using the strong electrostatic adsorption technique for stearic acid conversion via the deoxygenation process. *Appl. Nanosci.* **2021**, *11*, 2371−2381.
(42) Panagiotou, G. D.; Petsi, T.; Bourikas, K.; Garoufalis, Ch. S.; Tsevis, A.; Spanos, N.; Kordulis, C.; Lycourghiotis, A. Mapping the surface (hydr)oxo-groups of titanium oxide and its interface with an aqueous solution: The state of the art and a new approach. *Adv. Colloid Interface Sci.* **2008**, *142*, 20−42.


https://doi.org/10.1021/acs.langmuir.5c05228
*Langmuir* 2025, 41, 33586−33593